Members of the Arabidopsis auxin receptor gene family are essential early in embryogenesis and have broadly overlapping functions.

Michael J. Prigge, Nikita Kadakia[1], Kathleen Greenham[2], and Mark Estelle[*]

Section of Cell and Developmental Biology, University of California San Diego, La Jolla, California 92093-0116
[1] Current address: University of California, Riverside, School of Medicine, Riverside, California
[2] Current address: Department of Plant and Microbial Biology, University of Minnesota, Saint Paul, Minnesota, 55108

orcid.org/0000-0003-0671-2538 (MJP)
orcid.org/0000-0002-1884-1671 (NK)
orcid.org/0000-0001-7681-5263 (KG)
orcid.org/0000-0002-2613-8652 (ME)

ABSTRACT

The TIR1/AFB proteins are auxin co-receptors that mediate diverse responses to the plant hormone auxin. The genome of Arabidopsis encodes six TIR1/AFB proteins representing three of the four clades that were established prior to angiosperm radiation. To determine the role of these proteins in plant growth and development we have performed an extensive genetic analysis involving the generation and characterization of all combinations of multiply mutant lines. We find that loss of all six proteins results in defects in embryogenesis as early as the first division of the apical cell. Mutant embryos progress, but exhibit frequent errors in cell division and proliferation of the suspensor. Despite this dramatic phenotype, a single wild-type allele of *TIR1* or *AFB2* is sufficient to support growth of the plant throughout vegetative

development. Further, the TIR1/AFB pathway does not appear to be essential for development of the male or female gametophyte. Our analysis has revealed extensive functional overlap between even the most distantly related *TIR1/AFB* genes as well as examples of specialization.

INTRODUCTION

The phytohormone auxin regulates diverse processes throughout the entire plant life cycle. Auxin acts as a signal to promote cell differentiation during morphogenetic events such as embryogenesis, root development, and shoot organ formation. Auxin also mediates responses to environmental cues such as light, gravity, water availability, and pathogens. Auxin regulation of transcription involves three families of proteins; AUXIN RESPONSE FACTOR (ARF) transcription factors, Aux/IAA transcriptional repressors, and TRANSPORT INHIBITOR RESPONSE1 (TIR1)/AUXIN-SIGNALING F-BOX (AFB) proteins. Auxins, of which indole-3-acetic acid (IAA) is the predominant natural form, are perceived by a co-receptor complex consisting of TIR1/AFB and Aux/IAA proteins. Formation of the co-receptor complex leads to degradation of the Aux/IAA protein and activation of ARF-dependent transcription (Reviewed in (Lavy and Estelle 2016). In addition to this established pathway, recent studies demonstrate that the TIR1/AFB proteins are required for very rapid auxin responses that are independent of transcription (Dindas et al. 2018; Fendrych et al. 2018). The details of TIR1/AFB function in these rapid responses are currently unknown.

Members of the TIR1/AFB protein family are encoded by three pairs of ohnologs in the *Arabidopsis* genome. Each protein contains an amino-terminal F-Box followed by

eighteen leucine-rich repeats (LRRs). Only *tir1*, *afb2*, and *afb5* mutants have been identified in forward-genetic screens (Ruegger et al. 1997; Ruegger et al. 1998; Alonso et al. 2003; Walsh et al. 2006; Parry et al. 2009), but reverse-genetic analyses revealed functional redundancies between *TIR1*, *AFB2*, and *AFB3* as well as between *AFB4* and *AFB5*.

Gene duplication events provide the primary source material for the evolution of biological innovation. In plants, whole genome duplication (WGD) events have been especially important since events have preceded the radiation of several key plant lineages including seed plants, flowering plants, and core eudicots (Reviewed in (Clark and Donoghue 2018). Following duplication, the paralogs are often redundant, allowing one copy to degenerate into a pseudogene. In Arabidopsis, the average half-life of a duplicate gene has been estimated at 17.3 million years (Lynch and Conery 2003). In many cases, however, both duplicates are retained for one or a combination of reasons (reviewed in (Panchy et al. 2016). Occasionally, one of the paralogs evolves a novel function (neofunctionalization), but often the two paralogs fulfill different aspects (enzymatically, temporally, or spatially) of the role of the ancestral gene (subfunctionalization). Following subfunctionalization, there may be changes in selective pressure allowing each paralog to evolve specialized functions without affecting functions carried out by the other paralog. This mechanism likely played a prominent role in the evolution of plant gene families and, in turn, in the radiation and diversification of land plants.

The *TIR1/AFB*, *Aux/IAA*, and *ARF* gene families expanded during land plant evolution after the divergence of bryophytes and vascular plants (Remington et al. 2004;

Rensing et al. 2008). Because auxin has a central role in many important adaptations that occurred during land plant evolution, such as vascular development, lateral root formation, and organ polarity; it seems likely that the acquisition of new roles for auxin was enabled by the duplication and diversification of these three gene families. Here we present the comprehensive genetic analysis of the *TIR1/AFB* gene family of Arabidopsis which revealed extensive functional overlap between even distantly related members as well as an essential role for the TIR1/AFB pathway in early embryos.

RESULTS

Major lineages of auxin receptors diverged prior to fern-seed plant split

To better understand the timeframe during which the auxin receptor family diversified, we built upon previous phylogenetic analyses (Parry et al. 2009; Mutte et al. 2018) with more taxon sampling at key nodes. As shown earlier (Hori et al. 2014; Mutte et al. 2018), the *TIR1/AFB* genes likely evolved from a gene encoding an F-Box/LRR protein similar to those present in the genomes of extant streptophyte algae. These algal proteins form a sister clade to three distinct land plant F-Box families, the TIR1/AFB auxin receptors, the COI1 jasmonate-Ile (or dinor-OPDA) receptors, and the 'XFB' clade of unknown function conserved in the genomes of mosses and some lycophytes but not in other land plants (Bowman et al. 2018). While the last common ancestors of land plants and of vascular plants had only one *TIR1/AFB* gene, three clades of auxin receptors were established prior to the radiation of euphyllophytes (ferns plus seed plants) over 400 million years ago (Morris et al. 2018) (Figure 1—figure supplement 1A). Another gene duplication event prior to angiosperm radiation split the TIR1/AFB1 clade from the AFB2/AFB3 clade. Receptors from each of the four clades

are not retained in the genomes of all flowering plants. For example, *AFB6* orthologs are not present in the genomes of core Brassicales species—including Arabidopsis—nor those of Poaceae species. The gene duplication event establishing the distinct TIR1 and AFB1 clades is coincident with the At-β whole genome duplication (WGD) event at the base of Brassicales, while both the AFB2/AFB3 and the AFB4/AFB5 duplication events coincide with the more recent At-α WGD prior to divergence of the Brassicaceae family (Figure 1—figure supplement 1A) (Schranz and Mitchell-Olds 2006).

One noteworthy aspect of the phylogenetic tree is the pronounced branch-length asymmetry within the TIR1+AFB1 clade (Figure 1—figure supplement 1A and 1B). Since the last common ancestor of *Arabidopsis* (Brassicaceae) and *Tarenaya* (Cleomaceae), the *AFB1* gene has accumulated over three times as many non-synonymous changes as *TIR1* (Figure 1—figure supplement 1B) despite being under selection based on the ratio of non-synonymous and synonymous substitutions (Delker et al. 2010; Wright et al. 2017). AFB1 also differs from the other TIR1/AFBs in that it contains two of three substitutions in the first α-helix of the F-Box that were previously shown to weaken TIR1's interaction with CUL1 (Yu et al. 2015). The substitution with the largest effect, Glu8Lys (equivalent to Glu12Lys in TIR1), appeared shortly after the At-β WGD that produced AFB1, and the Phe14Leu substitution appeared prior to the crown group of the Brassicaceae family (Figure 1—figure supplement 1C). Interestingly, *AFB1* orthologs from members of the *Camelina* genus—*C. sativa* (all three homeologs), *C. laxa*, *C. hispida*, and *C. rumelica*—additionally contain the third substitution (Figure 1—figure supplement 1C).

Genetic Analysis of the *Arabidopsis TIR1/AFB* Gene Family

Previous studies have assessed the functional overlap between the *TIR1*, *AFB1*, *AFB2* and *AFB3* genes (Dharmasiri et al. 2005; Parry et al. 2009) and separately between the *AFB4* and *AFB5* genes (Prigge et al. 2016). To study the genetic interactions between all members of the family, and to determine the effects of the complete absence of the TIR1/AFB-mediated auxin signaling, lines with strong loss-of-function mutations in the six *TIR1/AFB* genes were intercrossed to generate all sixty-three mutant combinations. We used the following alleles *tir1-1, afb1-3, afb2-3, afb3-4*, *afb4-8*, and *afb5-5* (Figure 1—figure supplement 2A; (Ruegger et al. 1998; Parry et al. 2009; Prigge et al. 2016). The *tir1-1* allele, which causes an amino acid substitution within the leucine-rich repeat domain of the protein, has been reported to act as a dominant-negative allele (Dezfulian et al. 2016; Wright et al. 2017). However, we found that the root elongation phenotype of plants heterozygous for the *tir1-1*, *tir1-10*, and *tir1-9* alleles were not significantly different from each other and each displays a semi-dominant phenotype (Figure 1—figure supplement 2B). These results argue against a dominant negative effect for *tir1-1* since neither *tir1-9* or *tir1-10* produce significant levels of transcript (Ruegger et al. 1998; Parry et al. 2009). Nevertheless, because it is possible that a dominant-negative effect might be revealed in higher-order mutants and because the *afb2-3* allele may not be a complete null allele (Parry et al. 2009), we generated selected mutant combinations using the *tir1-10* (Parry et al. 2009) and the *afb2-1* (Dharmasiri et al. 2005) T-DNA insertion alleles. The *afb2-1* allele was introgressed from the Ws-2 background into the Col-0 background through at least eight crosses. For brevity, mutant line names will be simplified such that "*tir1afb25*"

corresponds to the *tir1-1 afb2-3 afb5-5* triple mutant line, for example, unless other allele numbers are specified.

The sixty-three mutant combinations displayed a wide range of phenotypes from indistinguishable from wild type to early-embryo lethality (Figure 1—figure supplement 3). The non-lethal higher-order mutant combinations displayed a cohort of phenotypes associated with mutants defective in auxin signaling: smaller rosettes, reduced inflorescence height, reduced apical dominance, fewer lateral roots, and partially or wholly valveless gynoecia (Figure 1; Figure 1—figure supplements 3 and 4). The three viable quintuple mutants—*tir1afb1245*, *tir1afb1345*, and *afb12345*—had rosettes approximately half the diameter and inflorescences less than half the height of WT Col-0. Despite being smaller, these lines produced approximately twice as many branches as WT (Figure 1A; Figure 1—figure supplement 4). Remarkably, lines retaining only one copy of *TIR1* (*tir1/+ afb12345*) or one copy of *AFB2* (*afb2/+ tir1afb1345*) were viable. The rosettes of these two lines were much smaller than those of WT plants with the *tir1/+ afb12345*'s rosette phenotype being slightly more severe (Figure 1B). In contrast, *afb2/+ tir1afb1345* plants developed shorter primary inflorescences and appeared to completely lack apical dominance as all axillary meristems became active upon flowering. The *afb2/+ tir1afb1345* and especially *tir1/+ afb12345* plants produced very few seeds, an average 0.6 and 14 seeds per plant, respectively (*n*=10 and 9). Lines containing the alternate alleles—*afb2-1/+ tir1-10 afb1345* and *tir1-10/+ afb2-1 afb1345*—displayed indistinguishable phenotypes (Figure 1B), although they tended to produce slightly more seed, 1.1 and 36 seeds per plant, *n*=18 and 8, respectively, so we cannot rule out a slight difference in allele behavior.

Auxin plays an important role in many aspects of root development. To begin to assess the role of the *TIR1/AFBs* during root growth, we measured the effect of exogenous IAA on primary root growth in the mutant lines. The response ranged from indistinguishable from WT to nearly insensitive to 0.5 μM IAA (Figure 1—figure supplement 4). As seen previously (Dharmasiri et al. 2005; Parry et al. 2009), the roots of lines containing the *tir1* and *afb2* mutations displayed strong IAA resistance. In addition, we found that the *afb3* and *afb5* mutations had substantial effects on auxin response, while the *afb4* mutation had a more modest effect. The mutant lines also responded similarly to exogenous auxin with respect to lateral root production. The lines with the strongest resistance to IAA in root elongation produced very few if any lateral roots (Figure 1—figure supplement 4).

Relative Gene Effects

Each of the *tir1/afb* mutations, except for *afb1*, affected the phenotypes that we scored but to various extents. To appraise the effects of each mutation on the phenotypes, we plotted the mean values for each phenotype minus that of the corresponding line without that mutation. Larger effects are indicated by greater deviations from zero. For both the root elongation assay and the induction of lateral root primordia, the *tir1* allele had the largest effect with the *afb2*, *afb5*, *afb3*, and *afb4* mutations having smaller median effects (Figures 2A and 2B). The *afb1* mutation had little or no effect on root elongation but surprisingly had an opposite effect on lateral root formation.

Only *tir1* and, to a lesser degree, *afb2* affect rosette diameter in most contexts with the median effects for *afb3*, *afb4*, and *afb5* being very close to zero (Figure 2C).

However, they have huge effects together: the *afb2345* quadruple mutant is over 6 cm smaller than each of the four triple mutants (arrowheads; Figures 2C). Consistent with previous reports that *AFB5* plays a key role in regulating inflorescence branching and height (Prigge et al. 2016; Ligerot et al. 2017), the *afb5* mutation has the largest effect on these phenotypes, although each mutation, except for *afb1*, had some effect (Figures 2D and 2E).

While the *afb1* mutation had minimal effect on most aspects of plant growth, it suppressed the lateral root phenotype of some mutant lines both with and without auxin treatment (Figure 2B; below). We found that the *afb1* mutation suppressed the phenotype of both the *afb234* (2.15±0.13 versus 1.75±0.10 lateral roots/cm) and *afb345* triple mutants (3.10±0.13 versus 1.96±0.14 lateral roots/cm) measured after 12 days on media not supplemented with IAA. This behavior was not observed in an otherwise WT background (2.76±0.11 for *afb1* versus 3.23±0.15 lateral roots/cm for Col-0) nor in a *tir1-1* background (1.75±0.08 versus 2.34±0.09 lateral roots/cm for *tir1*). Each of the pairs were significantly different (two-tailed *t*-test, $P < 0.03$).

Defects in Embryonic Root Formation

The *tir1afb23* and *tir1afb123* lines were previously shown to display a variably penetrant phenotype in which seedlings lack roots, lack both roots and hypocotyls, or fail to germinate (Dharmasiri et al. 2005; Parry et al. 2009). All lines homozygous for both *tir1* and *afb2* plus either *afb3*, *afb4*, or *afb5* display these defects to some degree ranging from 1% in *tir1afb24* to 99% in *tir1afb1234* (Figure 1—figure supplements 3 and 5).

We had noticed a sizeable difference in the proportion of seedlings lacking roots from different batches of seeds. To test whether the temperature at which the seeds mature affects the penetrance of the rootless seedling phenotype, we grew *tir1afb23*, *tir1afb123*, *tir1afb245* and WT in parallel at 17°C, 20°C, and 23°C and scored the progeny seedling phenotypes (Figure 1—figure supplement 5). The penetrance of the phenotype for all three lines was significantly lower at 20°C than at either 17°C or 23°C for all with the exception that the difference with *tir1afb245* at 17°C was not significant using the Fisher's exact test. This suggests that aspects of the auxin regulatory system are sensitive to temperature.

Early-Embryo Defects of the *tir1afb235* and *tir1afb12345* mutant lines

Because *tir1afb235* seedlings were not identified among the progeny of *tir1/+ afb235* or *afb2/+ tir1afb35* plants, we examined developing embryos in the siliques from these lines. Roughly one-quarter of the embryos from each line lacked cotyledons and had over-proliferated suspensors while the rest had a WT phenotype (Figure 3A–3B). Identical defective embryos were seen for lines additionally homozygous for the *afb1* mutation (Figure 1—figure supplement 3). Because all mutant combinations that we expected to produce one-quarter *tir1afb2345* or *tir1afb12345* progeny were either seedling lethal or infertile, we looked at the progeny of plants that were heterozygous at two loci: *tir1/+ afb2/+ afb345*, *tir1/+ afb2/+ afb1345*, and *tir1/+ afb5/+ afb1234*. We observed embryos indistinguishable from those seen for the *tir1afb235* quadruple mutant at a rate close to the expected 1/16 ratio.

To facilitate a more detailed analysis of the sextuple mutant, we assembled the complementing genomic fragments encoding TIR1, AFB2, and AFB5, each carboxy-

terminally fused with the coding sequences for different monomeric fluorescent proteins (mOrange2, mCitrine, and mCherry, respectively) into a single locus (Figure 3—figure supplement 1). This construct was transformed into *afb1234* plants, crossed into a sextuple mutant background, and two *TO/5Ch/2Ci* lines were identified that complemented the sextuple mutant phenotype when hemizygous and segregated as a single locus. Using this approach, one-quarter of the progeny of plants hemizygous for these transgenes display embryo defects, while the complemented siblings are easily identified because they expressed fluorescent TIR1, AFB2, and AFB5 fusion proteins.

The first discernable difference between sextuple mutants and the complemented siblings is that the initial division of the embryo proper was displaced from vertical in nearly half of the sextuple 2-cell embryos (6 of 15) compared to only one slightly skewed division out of 18 sibling embryos (Figure 3C–F). Later, during the transition from the 8-cell to the 16-cell embryos, nearly all cell divisions in the complemented embryos are oriented periclinally, as in WT embryos. In contrast, most of these division are anticlinal in the mutant embryos (Figure 3I–J). In WT 32-cell stage embryos, the hypophysis cell normally divides asymmetrically to produce the lens-shaped cell which is required for the formation of the embryonic root. This division was delayed in the mutant, and when it occurred, was symmetrical (Figure 3M–P). Later, the cells of the embryo proper slow or cease dividing and the cells of the suspensor begin to proliferate (Figure 3Q–X). Around the stage where complemented siblings are at the bent-cotyledon stage, the cells of the sextuple mutant produce cytoplasmic autofluorescence, likely indicating senescence, and seed development is aborted.

Marker gene expression in *tir1afb235* quadruple mutant embryos

To learn more about the early embryo defects, we introgressed marker genes into lines segregating the *tir1afb235* quadruple mutant. Expression of the auxin-responsive marker $DR5_{rev}$*:3×Venus-N7* was undetectable in embryos displaying the mutant phenotype (Figure 4E–G; compare to Figure 4A–C) indicating that auxin perception through AFB4 and AFB1 is minimal during embryogenesis. The *NTT-YPet* marker gene is normally first strongly expressed in 8- to 16-cell embryos in the nuclei of suspensor cells and the hypophysis and persists in the suspensor and the hypophysis-derived cells in later embryo stages (Figure 4R–T)(Crawford et al. 2015). In mutants, NTT-YPet appears normally in the suspensor cells, but not in the hypophysis, and is progressively lost in the distal suspensor cells before the abnormal lateral cell divisions occur (Figure 4V–X) . *PIN7-Venus* is also normally expressed in the suspensor, hypophysis, and hypophysis-derived cells (Figure 4K–L). In mutant embryos, PIN7-Venus is faintly detectable in these cells in early-globular embryos. Unexpectedly, the signal is stronger in the lower tier of the embryo proper, starting at the late-globular stage (Figure 4O–P). The same pattern was observed with the *PIN7-GFP* marker (Figure 4U). The *PIN1-Venus* marker initially is expressed in a reciprocal pattern to *PIN7-Venus*, in all the cells above the hypophysis and is later refined to strips from the provascular cells out to the cotyledon tips (Figure 4I–J). In the mutants, PIN1-Venus appears faintly in early embryos and never resolves to specific cell types in later embryos (Figure 4M–N). The *WOX5:GFP* marker is first expressed in the hypophysis prior to its asymmetric division then persists in the quiescent center cells (Figure 4D). No WOX5:GFP signal was detected in the mutant embryos (Figure 4H).

Viability of sextuple mutant gametophytes

Because the maternal supply of auxin and the endosperm both play important roles in embryo development, it is possible that female gametophytes lacking auxin receptors would not be viable. That we were able to identify sextuple mutant embryos shows that the gametophytically-expressed auxin receptors are not completely required, but it is possible that they are required for robust transmission. To test the transmission through sextuple mutant megagametophytes and pollen, we carried out reciprocal crosses between wild type (Col-0) and lines homozygous for four loci and heterozygous for the other two (*tir1/+ afb2/+ afb1345*, *tir1/+ afb5/+ afb1234*, *afb2/+ afb5/+ tir1afb134*, and *afb2/+ afb4/+ tir1afb135*) and then determined the genotypes of all the progeny (Figure 3—figure supplement 2). When the *tir1/afb* mutant lines are used as the pollen donor, approximately one-quarter of the progeny were heterozygous at all six loci indicating that transmission of sextuple mutant pollen is not discernably different from non-sextuple pollen. When the *tir1/afb* lines were used as the female parent, though, we detected fewer than the expected number of progeny that are heterozygous at all six loci, although the deviation was not highly significant (χ^2 = 3.74, P=0.053, for the four populations combined). Thus, gametophytically expressed TIR1/AFBs may contribute to megagametophyte viability but are not essential.

TIR1/AFB protein expression

To see if differences in expression patterns can account for the differences in relative importance of the TIR1/AFBs in different aspects of growth and development, C-terminal fusions with the bright, relatively fast-folding, monomeric fluorescent protein mCitrine were produced for each TIR1/AFB protein in the corresponding single mutant

background. The fluorescent signal in the *AFB5-mCitrine* lines was fairly uniformly distributed in shoot apices (Figure 5F), while in the *AFB3-mCitrine*, *AFB2-mCitrine*, and *TIR1-mCitrine* lines, fluorescence was more restricted to young primordia and meristem peripheral zones (Figure 5A, 5C–D). Within organ primordia, *TIR1-mCitrine* appears to be strongest in the adaxial domains of the youngest primordia. Signal for the *AFB4-mCitrine* line was barely detectable (Figure 5E), while that of *AFB1-mCitrine* was very strong and largely complementary to *TIR1-mCitrine* in that the strongest signal was in abaxial domains and in the stem (Figure 5B). In roots, TIR1-, AFB2-, AFB3-, and AFB5-mCitrine signal was uniformly detected throughout the root meristematic region and fainter signal detected in the root cap cells (Figure 5G, 5I–J, 5L; Figure 5—figure supplement 1). AFB1-mCitrine is very highly expressed throughout the root except for the columella, cortex, endodermis, and pericycle of the meristematic region (Figure 5H). AFB4-mCitrine signal in lines that complemented the *afb4* phenotypes was barely detectable, although a picloram-hypersensitive line's expression pattern was comparable to that of AFB5-mCitrine (Figure 5K; Figure 5—figure supplement 1I–M). In embryos, TIR1-, AFB2-, AFB3-, and AFB5-mCitrine accumulate fairly uniformly throughout the embryos and suspensors while AFB4-mCitrine's signal was close to background levels and AFB1-mCitrine was undetectable (Figure 5M–R). The subcellular localization appeared to differ between the different TIR1/AFB proteins, especially in root cells (Figure 5G–L; Figure 5—figure supplement 1). TIR1-mCitrine appears almost exclusively in nuclei while AFB1-mCitrine appears almost exclusively outside the nuclei. The other four AFB protein fusions appear to be primarily localized to nuclei but with a significant amount of signal elsewhere. The localizations are consistent across multiple

lines and, in some cases, different fluorescent protein tags (Figure 5—figure supplement 1).

DISCUSSION

The TIR1/AFB protein family has expanded through a series of gene duplication events that began before fern–seed-plant divergence. Despite the fact that three major subclades were established approximately 400 MYA (Morris et al. 2018), our genetic studies reveal that the TIR/AFB proteins retain largely overlapping functions, at least during standard growth conditions. In general, *TIR1* is most important for normal growth and development, but *AFB5* and *AFB2*, and to a lesser extent *AFB3* and *AFB4*, also play significant roles. Spatial differences are also apparent; *TIR1* has a major role in the root while *AFB5* is relatively more important in inflorescence development.

Although all six genes are broadly expressed, it seems likely that differences in the relative importance of individual TIR1/AFB proteins in various organs are at least partly related to differences in expression. For example, *AFB5* is more broadly expressed than the other genes in the inflorescence while in the root, *TIR1* and *AFB2* are most highly expressed. The *AFB4* gene is expressed at a lower level in all tissues consistent with its relatively minor role. Additional differences in patterns of expression are also apparent, particularly in the inflorescence. Further studies will be required to determine if these differences are important.

Our studies demonstrate that the levels of the TIR1/AFB proteins are not uniform throughout the plant. This is true for individual members of the family and for total TIR1/AFB levels across different tissues and cell types. Earlier experiments also showed that TIR1/AFB levels can be dynamic in a changing environment (Wang et al.

2016). These observations may have important implications for use of DII-Venus-based auxin sensors to estimate relative auxin levels, since levels of the sensor protein are dependent on both auxin and the TIR1/AFBs (Brunoud et al. 2012; Liao et al. 2015).

It is important to emphasize that individual members of the family may have specialized functions in particular environmental conditions. For example, the microRNA *miR393* is known to target *TIR1, AFB2*, and *AFB3* but not other members of the family (Jones-Rhoades and Bartel 2004; Navarro et al. 2006). Regulation of miR393 abundance modulates the levels of these three TIR1/AFBs to facilitate various growth processes, such as lateral root formation and hypocotyl elongation in response to environmental signals (Vidal et al. 2010; Pucciariello et al. 2018).

Previous *in vitro* studies have documented some differences in the biochemical activity of members of the TIR1/AFB family (Calderón Villalobos et al. 2012; Lee et al. 2014). Similarly, an auxin-induced degradation assay in yeast reveals differences in the behavior of TIR1 and AFB2 (Wright et al. 2017). In contrast, our results do not reveal any biochemical specificity, except for *AFB1* (see below). Thus, a single *TIR1* or *AFB2* allele is sufficient to support viability throughout the plant life cycle albeit with dramatically reduced fertility. This contrasts to functional diversification seen in other well-studied gene families that diverged in a similar time frame such as the phytochrome photoreceptors and Class III HD-Zip transcriptional regulators (Prigge et al. 2005; Franklin and Quail 2010; Strasser et al. 2010). It is possible that the retention of overlapping functions reflects stricter constraints on TIR1/AFB protein function. One possibility is that the different TIR1/AFB paralogs have been maintained because they

contribute to the robustness of the auxin signaling system. Of course, specific functions may be revealed in future studies.

The AFB1 protein is unique among the auxin co-receptors and may have undergone neofunctionalization during the early diversification of the Brasssicales order. Although AFB1 can interact with Aux/IAA proteins in an auxin-dependent manner, it is not able to efficiently assemble into an SCF complex and is not primarily localized in the nucleus where it could directly influence transcriptional responses (Yu et al. 2015)(Figure 5H; Figure 5—figure supplement 1C–D). If it is acting as a typical auxin co-receptor, it would likely be very inefficient and might only have a discernable effect at high auxin concentrations when the other receptors are saturated. Alternatively, AFB1 may negatively regulate the other members of the family through its ability to sequester auxin, Aux/IAAs, ASK1 and/or other TIR1/AFB-interacting partners. For example, at high auxin concentrations, AFB1 may act to reduce the level of auxin available to the other active co-receptors. It is noteworthy that unlike the other *TIR1/AFB* genes that are broadly expressed in most cells, *AFB1* is expressed very highly in some tissues (root epidermis and vascular tissue) and not at all in others (meristematic pericycle). Based on our genetic studies, AFB1 appears to have a negative effect on lateral root initiation in the *afb234* and *afb345* lines despite the fact that AFB1 is not expressed in the pericycle. Perhaps AFB1 sequesters auxin that is flowing through the epidermis or stele and limits the amount of auxin that reaches the pericycle.

Most of TIR1 and AFB2 through AFB5 are localized to the nucleus as expected, but we also observe some protein present in the cytoplasm. The significance of this localization is unknown. Perhaps cellular Aux/IAA pools are regulated in part through

degradation in the cytoplasm. One intriguing possibility is that cytoplasmic co-receptors are important for the recently described very rapid auxin responses in the root (Dindas et al. 2018; Fendrych et al. 2018).

The importance of auxin in patterning of the developing embryo is well established (Palovaara et al. 2016). Auxin signaling, as evidenced by activity of the *DR5* reporter, is first apparent in the apical cell of the embryo (Friml et al. 2003). The essential role of auxin in the apical cell and later in the hypophysis is clearly demonstrated by the defects in the division of these cells in the *tir1afb235* quadruple and *tir1afb12345* sextuple mutant (Figure 3). Similar defects are observed in a number of other auxin mutants including those affecting response (*monopteros* and *bodenlos*), auxin synthesis (*yuc1 yuc4 yuc10 yuc11* and *taa1 tar1 tar2*) and transport (*pin1 pin3 pin4 pin7* and *aux1 lax1 lax2*)(Berleth and Jürgens 1993; Hardtke and Berleth 1998; Hamann et al. 1999; Hamann et al. 2002; Friml et al. 2003; Cheng et al. 2007; Stepanova et al. 2008; Robert et al. 2015). However, none of these lines exhibit the fully penetrant embryo-lethal phenotype observed for the *tir1afb235* quadruple and *tir1afb12345* sextuple mutants. In the other mutants, a significant fraction of embryos escape embryo lethality and germinate, albeit often as rootless seedlings.

The expression of key embryonic markers in the mutants also reveals profound defects in embryonic patterning by the dermatogen stage. Although *tir1afb235* embryos form a morphologically normal hypophysis cell, this cell never expresses *NTT-YPet* or *WOX5:GFP.* The proliferation of suspensor cells in the mutant is associated with reduced expression of the suspensor marker *PIN7-Venus* and to a lesser extent *NTT-YPet* suggesting that the TIR1/AFB pathway is required to maintain the suspensor cell

fate, consistent with an earlier study (Rademacher et al. 2012). *PIN1-Venus* is expressed in the globular embryo distal from the hypophysis in *tir1afb235* mutants as in WT, but none of the dynamic changes related to cotyledon and provascular tissue specification occur. It was surprising to observe that *PIN7-Venus* exhibits ectopic expression in the basal half of the embryo proper. The reason for this is obscure but one possibility is that *PIN7* expression is normally repressed in the embryo by a TIR1/AFB-dependent pathway.

METHODS

Phylogeny

The sources for the amino-acid sequences (Figure 1—figure supplement 1A) and CDS (Figure 1—figure supplement 1C) are listed in Supplementary File 1 (Goodstein et al. 2012; Johnson et al. 2012; Matasci et al. 2014; Wickett et al. 2014; Xie et al. 2014). Taxa were selected based on availability, quality, and diverse sampling at key nodes. A reduced set were included for COI1 homologs. The *AFB1* genes from *Camelina hispida*, *C. laxa*, and *C. rumelica* were amplified from genomic DNA using Phusion Polymerase (New England Biolabs or ThermoFisher) and primers to regions of the 5′ and 3′ UTRs conserved in all three *C. sativa AFB1* genes. The PCR products were subcloned, and three *C. hispida* and *C. laxa* clones and a single *C. rumelica* clone were sequenced. The *CamhiAFB1* and *CamlaAFB1* sequences included in analysis appeared in two of the three clones (GenBank accession numbers MK423960–MK423962).

To build the alignment of F-Box-LRR protein sequences, sequences from distinct subclades were aligned using T-COFFEE (Notredame et al. 2000) to identify and trim unique unalignable regions from individual sequences before aligning the whole set. Ambiguous regions of the full alignments were removed in Mesquite (Maddison and Maddison 2018). The raw alignment of nucleotide CDS sequences of Brassicales *TIR1/AFB1* genes were adjusted so that gaps fell between adjacent codons. Phylogenetic trees were inferred using MrBayes (Ronquist et al. 2012). For the TIR1/AFB/XFB/COI1 phylogeny, a total of six runs of four chains were split between two Apple iMac computers using the parameters aamodelpr=mixed, nst=6, and rates=invgamma. Only four of the six runs had converged after 16 million generations, so the analysis was restarted with three runs each starting with the best tree from one of the initial runs and with more heating (temp=0.5) for 10 million generations. The *TIR1/AFB1* nucleotide alignments were partitioned by codon position with ratepr = variable, nst = 6, rates = invgamma with three runs of 4 chains run for five million generations. The consensus trees were viewed using FigTree v1.4.4 (Rambaut 2018).

Mutants

The alleles used—*tir1-1, tir1-9, tir1-10, afb1-3, afb2-1, afb2-3, afb3-1, afb3-4, afb4-8, and afb5-5*—have been described previously (Ruegger et al. 1998; Dharmasiri et al. 2005; Parry et al. 2009; Prigge et al. 2016). Seeds from *Camelina* species were provided by the United States National Plant Germplasm System (USDA-ARS, USA): *C. hispida* (PI 650133), *C. laxa* (PI 633185), and *C. rumelica* (PI 650138). Unless noted, plants were grown at 22°C long-day (16:8) conditions on ½× Murashige and Skoog media with 0.8% agar, 1% sucrose, and 2.5 mM MES, pH 5.7, or in a 2:1 mixture of soil

mix (Sunshine LC1 or ProMix BX) and vermiculite. Leaf DNA was isolated with a protocol adapted from (Edwards et al. 1991) to use steel BBs (Daisy Outdoor Products), 2 ml microcentrifuge tubes, and 20-tube holders (H37080-0020, Bel-Art). See Supplementary File 2 for primers used for genotyping.

Fluorescent marker lines were described previously: *NTT-2×YPet* (Crawford et al. 2015), *PIN7-GFP* (Blilou et al. 2005), *DR5rev:3×Venus-N7* (Heisler et al. 2005), *WOX5:GFP*$_{ER}$ (Blilou et al. 2005). The recombineered *PIN1-Venus* and *PIN7-Venus* markers (Zhou et al. 2011) were obtained from the Arabidopsis Biological Resource Center (CS67184 and CS67186). Previously characterized *PIN1-GFP* lines could not be used because of tight linkage to *AFB2* (CS9362) and co-segregation with enhancers of the *afb2/+ tir1afb35* phenotype (CS23889). Each marker was introgressed into lines segregating the *tir1afb235* quadruple mutant by two sequential crosses, PCR genotyping, and selfing. Marker line homozygousity was confirmed in F_1 seedlings from test crosses to WT.

Fluorescently tagged TIR1/AFB lines

Genomic regions containing each of the *TIR1/AFB* genes were amplified using Phusion polymerase (New England Biolabs or ThermoFisher) from corresponding genomic clones (JAtY51F08, JAtY62P14, JAtY53F15, JAtY61O12, and JAtY52F19) except for *AFB3* which was amplified from Col-0 genomic DNA. See Supplementary File 2 for primers used. The PCR products were cloned into pMiniT (New England Biolabs), and the stop codon was altered to create a *Nhe*I site using site-directed mutagenesis. An *Xba*I fragment containing either mCitrine (Griesbeck et al. 2001), mOrange2 (Shaner et al. 2008), or mCherry (Shaner et al. 2004) preceded by a short linker (either Arg-Gly$_5$-

Ala or Arg-Gly_4-Ala) was ligated into the *Nhe*I sites. The genomic regions including the fluorescent protein genes were inserted in the *Mlu*I site of pMP535 (Prigge et al. 2005) as *Asc*I fragments (*AFB5*) or as *Mlu*I-*Asc*I fragments (others). To produce the sextuple-complementation construct, the *TIR1-mOrange2* fragment was cloned into pMP535 as above, then *AFB2-mCitrine* was inserted into the re-created *Mlu*I site followed by *AFB5-mCherry* into its re-created *Mlu*I site. The constructs were introduced into the following strains by floral dip (Clough and Bent 1998): *tir1/+ afb5/+ afb1234* progeny (sextuple-complementation construct), *tir1afb23* (*TIR1-mCitrine* and *AFB3-mCitrine*), *tir1afb1245* (*AFB2-mCitrine*), *afb45* (*AFB4-mCitrine*), *afb5-5* (*AFB5-mCitrine*, and *afb1-3* (*AFB1-mCitrine*). Basta-resistant candidate lines were selected based on complementation phenotypes (except for *AFB1-mCitrine*) then crossed to get them into the appropriate mutant backgrounds. Once in the sextuple-mutant background, the complementation transgene was maintained as a hemizygote by checking siliques for aberrant embryos or aborted seeds. The *afb5-5 AFB5-mCitrine #9* and *#19* lines were described previously (Prigge et al. 2016).

Microscopy

For confocal microscopy of the root meristem, five- to seven-day-old seedlings were stained in a 10 µg/ml aqueous solution of propidium iodide for one minute, rinsed in water, mounted with water, and viewed with either a Zeiss LSM 880 inverted microscope or a Zeiss LSM 710 inverted microscope. Embryos were fixed and stained with SCRI Renaissance 2200 (SR2200; Renaissance Chemicals, UK; (Crawford et al. 2015). Briefly, using fine forceps and a 27-gauge needle as a scalpel, developing seeds were dissected from siliques and immediately immerged in fix solution (1×PBS, 4%

formaldehyde (Electron Microscopy Sciences, 15713), and 0.4% dimethyl sulfoxide) in a six-well plate with 100µ-mesh strainers. A vacuum was pulled and held three times for 12 minutes each time, before rinsing twice with 1×PBS for 5 minutes. The embryos were transferred to SR2200 stain [3% sucrose, 4% diethylene glycol, 4% dimethyl sulfoxide and 1% SR2200 and stained overnight with vacuum pulled and released 3-4 times. Seeds were mounted (20% glycerol, 0.1×PBS, 0.1% dimethyl sulfoxide, 0.1% SR2200, and 0.01% Triton X100) and the embryos were liberated by pressing on the coverslip. To detect mCitrine in the shoot apices, we removed stage 5 and older floral buds using fine forceps, fixed and rinsed (as with the embryos), soaked in ClearSee (Kurihara et al. 2015) for seven to ten days changing the solution every two to three days, and then stained with basic fuchsin (not shown) and Fluorescent Brightener 28 (Calcofluor White M2R) as described (Ursache et al. 2018). Confocal image channels were merged using ImageJ or FIJI (Schindelin et al. 2012; Schneider et al. 2012). Cleared embryos were viewed by mounting dissected ovules in a solution containing 2.5 g chloral hydrate dissolved in 1 ml 30% glycerol and viewing with a Nikon E600 microscope.

Phenotype comparisons

The viable *tir1afb* lines were divided based on whether they contained the *tir1* mutation, and the two batches were grown sequentially. The *afb123* line included in the initial batch was noticed to display a long-hypocotyl phenotype that may have been picked up after an earlier cross to the *afb4-2* mutant, so a third batch was made up of alternative isolates for five lines whose pedigrees included a cross to *afb4-2*. Each batch included Col-0 and *tir1-1*. Seeds were surfaced sterilized, stratified in water for

five days, spotted onto ½ MS medium containing 1% sucrose, and incubated in a light chamber (22°C). Twelve five-day-old seedlings for each genotype were transferred to 120 mm square plates containing the same medium containing either 0, 20, or 100 nM IAA (batch a), 0, 100, or 500 nM IAA (batch b), or 0, 20, 100, or 500 nM IAA (batch c). Each plate received six seedlings from six genotypes spread out over two rows. Seedlings for each genotype were present on the top row of one plate and the lower row on a second plate placed in a different part of the growth chamber after marking the position of the root tips with a marker and scanning with Epson V600 flatbed scanners. The plates were scanned again after 72 hours, and the growth during the 72 hours was measured using imageJ. The plates containing 100 nM IAA were grown for a fourth day before the numbers of lateral roots protruding through the epidermis were counted using a dissecting microscope. Five seedlings from the no-IAA control plates were transferred to soil in 6cm pots and grown an additional 34 days. The genotypes for two plants per line were confirmed by PCR. For each 42-day-old plant, the height from the rosette to the tip of the longest inflorescence and the maximum rosette diameter were measured, and the numbers of branches of at least 1 cm were counted. The IAA effects on root elongation data is presented as the percent relative to the growth without IAA ± the relative standard error of the ratio. For the gene effect analyses, the averages from each batch were normalized using measurements for Col-0 and *tir1-1* plants that were included with each batch.

ACKNOWLEDGMENTS

We thank Yingluo Wang, Diane Le, and Whitnie Szutu for technical assistance; Yi Zhang and Brian Crawford for help with microscopy; and the Arabidopsis Biological

Resource Center and the US National Plant Germplasm System for seeds. This work was supported by a grant from the NIH (GM43644 to ME). NK was supported in part through a UC San Diego Biological Sciences Eureka Summer Research Scholarship.

FIGURES AND TABLES

Figure 1. *tir1/afb* mutant lines exhibit a range of shoot phenotypes. (**A**) The viable quintuple mutants, *tir1afb1245, tir1afb1345*, and *afb12345,* are each approximately half the height of Col-0 WT, but differ in other phenotypes. Note the curved silique tips of the *tir1afb1245* mutant (indicative of gynoecium defects) and the short siliques (due to poor fertility) of the *afb12345* mutant. (**B**) Lines with only one *TIR1+* or one *AFB2+* allele display similar phenotypes regardless of the mutant *tir1* and *afb2* alleles: left to right, *tir1-1/+ afb2-3 afb1345*, *tir1-1 afb2-3/+ afb1345*, *tir1-10/+ afb2-1 afb1345*, and *tir1-10 afb2-1/+ afb1345*. (**C**) Normal siliques (Col-0, left) have two valves containing developing seeds while siliques of *afb2/+ tir1afb35* plants usually lack one (middle) or both valves (right). Plants were grown for 42 days (A and B) or 39 days (C) at 22°C and 16h daylength.

Figure 2. Relative *TIR1/AFB* gene effects. For each of the five phenotype measurements (Figure 1—figure supplement 4), the normalized mean for each genotype with the given mutation was subtracted from the normalized mean for the corresponding genotype lacking that mutation and plotted (circles). The red bars indicate the median difference attributable to the given mutation. (**A**) Effects of each mutation on IAA-inhibition of root elongation. For each genotype, twelve five-day-old

seedlings were transferred and grown for three days on media containing 100 nM IAA, and their average growth was divided by that of twelve seedlings grown on media lacking added auxin. (**B**) Effects of each mutation on auxin-induced lateral root production. Twelve five-day-old seedings for each genotype were grown for four days on media containing 100 nM IAA and the numbers of emerged lateral roots were counted. (**C**) Effects of each mutation on the average rosette diameters of five 42-day old plants. The blue arrowheads indicate difference in phenotypes between the *afb2345* quadruple mutant and the four triple mutants, and the green arrowheads indicate those for the *afb12345* quintuple mutant and the five quadruple mutants. (**D**) Effects of each mutation on the average height of the primary inflorescences for five 42-day old plants. (**E**) Effects of each mutation on the average number of inflorescence branches (≥1 cm) on five 42-day old plants. (**F**) Representation of the relative gene effects based on panels **A** through **E** plus embryo phenotypes (below). The line weights reflect the relative importance for each gene's roles. The red line with the bar end indicates the antagonistic role observed for *AFB1*.

Figure 3. Embryo-lethal phenotypes of *tir1/afb* mutant lines. Approximately one-quarter of the chloral-hydrate-cleared embryos from siliques of *afb2/+ tir1afb35* plants did not produce cotyledon primordia and have over-proliferated suspensors (**A**) while the remaining siblings from the same silique appear normal (**B**). Embryos from *TO/5Ch/2Ci#d2/+ tir1afb12345* (**C**–**O, R**–**Z**) and *TO/5Ch/2Ci#d1/+ tir1afb12345* (**P**–**Q**) plants were fixed, stained with SR2200 (cell walls, magenta), and scanned for fluorescence from the AFB2-mCitrine fusion protein (yellow). The embryos in panels **C**,

D, **G**, **I**, **K**, **M**, **O**, **Q**, **S**, **U**, **W**, and **Y** are sextuple mutants lacking mCitrine signal while those in **E**, **F**, **H**, **J**, **L**, **N**, **P**, **R**, **T**, **V**, **X**, and **Z** are complemented siblings. The embryo stages are 2-cell (**C**–**F**), 8-cell (octant) (**G**–**H**), 16-cell (dermatogen) (**I**–**J**), early globular (**K**–**L**), late globular (**M**–**P**), late transition (**Q**–**R**), heart (**S**–**T**), torpedo (**U**–**X**), and bent cotyledon (**Y**–**Z**). The cytoplasmic signal in panels **S**, **W**, and **Y** likely represents autofluorescence of senescing cells.

Figure 4. Marker gene expression in the *tir1afb235* embryos. Fluorescence in embryos from both *afb2/+ tir1afb35 DR5rev:3×Venus-N7* (**A**–**C, E**–**G**) and *afb2/+ tir1afb35 WOX5:GFP*$_{ER}$ (**D**, **H**) markers was present in phenotypically normal siblings (**A**–**D**) but absent in abnormal (presumed *tir1afb235*) embryos (**E**–**H**). Fluorescence in embryos from *tir1/+afb235 PIN1-Venus* plants: normal-phenotype globular embryo (**I**), normal-phenotype torpedo-stage embryo (**J**), mutant-phenotype globular embryo (**M**) and later-stage embryo (**N**). Progeny of *tir1/+ afb235 PIN7-Venus* or *afb2/+ tir1afb35 PIN7-GFP* plants: phenotypically normal globular embryos (**K**, **Q**) mutant globular embryos (**O**, **U**), and normal (**L**) and mutant (**P**) torpedo-stage embryos. Progeny of *afb2/+ tir1afb35 NTT-YPet* plants: normal-phenotype globular- (**R**–**S**) and transition- (**T**) stage embryos, and mutant embryos (**V**–**X**). Scale bars: 10 μm.

Figure 5. Expression of *TIR1/AFB-mCitrine* fusions. mCitrine signal is shown as yellow in all panels, and cell walls were stained with Calcofluor White M2R (blue; **A**–**F**), propidium iodide (magenta; **G**–**L**), and SCRI Renaissance 2200 (blue; **M**–**R**). Confocal images of inflorescence apices from 4-week-old plants containing the specified

TIR1/AFB-mCitrine transgenes in the corresponding single-mutant background: **A**, *tir1-10 TIR1-mCitrine#2*; **B**, *afb1-3 AFB1-mCitrine#7*; **C**, *afb2-3 AFB2-mCitrine#3*; **D**, *afb3-4 AFB3-mCitrine#1*; **E**, *afb4-8 AFB4-mCitrine#3*; and **F**, *afb5-5 AFB5-mCitrine#19*. Confocal images of roots of *tir1-10 TIR1-mCitrine#2* (**G**), *afb1-3 AFB1-mCitrine#7* (**H**), *afb2-3 AFB2-mCitrine#3* (**I**), *afb3-4 AFB3-mCitrine#1* (**J**), *afb4-8 AFB4-mCitrine#1* (**K**), and *afb5-5 AFB5-mCitrine#23* (**L**) 5-day old seedlings. Images in panels **G** and **J**–**L** used similar microscope settings while those in panels **H** and **I** used less sensitive settings. Confocal images of dermatogen or early globular embryos of *tir1-10 TIR1-mCitrine#2* (**M**), *afb1-3 AFB1-mCitrine#7* (**N**), *afb2-3 AFB2-mCitrine#3* (**O**), *afb3-4 AFB3-mCitrine#1* (**P**), *afb4-8 AFB4-mCitrine#3* (**Q**), and *afb5-5 AFB5-mCitrine#19* (**R**) plants. Scale bars equal 25 μm (**A**–**F**), 50 μm (**G**–**L**), and 10 μm (**M**–**R**).

Figure 1—figure supplement 1. TIR1/AFB Phylogeny. (**A**) The MrBayes-inferred gene tree illustrates the relationships between three F-Box-LRR protein families in land plants. The sources of the sequences are indicated by tip label colors: *Arabidopsis thaliana*, black; other eudicots, gray; monocots, light blue; magnoliids, dark blue; ANITA grade angiosperms, dark purple; gymnosperms, brown; ferns, red; lycophytes, light purple; mosses, dark green; liverworts, teal; hornworts, tan; and algae, light green. Three clades of TIR1/AFB proteins have well-supported fern sister clades indicating that first gene duplications in the family predated euphyllophyte radiation. Note that the position of the lycophyte TIR1/AFBs relative to those of bryophytes and seed plants was not resolved. (**B**) The graph shows the sum of branch lengths (amino-acid substitutions per site) from the node joining the Cleomaceae and Brassicaceae clades to the tip for

the Arabidopsis member of the clade. (**C**) Gene tree for the TIR1 and AFB1 clades with the parsimoniously inferred relative dates for the appearance of the three substitutions in the first helix of the F-Box that were shown to interfere with SCF assembly. The *Salvadora AFB1* transcript assembly lacked the sequence encoding this helix so that ancestor's sequence could not be predicted.

Figure 1—figure supplement 2. Alternate *tir1/afb* alleles. **A**, Diagram of exon/intron structure showing the locations of each mutation used in this study. T-DNA insertions are shown as triangles with the arrowheads indicating the locations of left-border sequences. The box in the third exons indicates the regions targeted by miR393. **B**, Root elongation inhibition assay of seedlings homozygous or heterozygous (F_1 progeny of Col-0 crosses) for three *tir1* alleles. P-values: *, ≤0.05 and **, ≤0.005 compared to Col-0; °, ≤0.05 and °°, ≤0.005 compared to *tir1-10*; and †, ≤0.05; ††, ≤0.005 compared to *tir1-10*/+. **C**, 32-day old Col-0, *afb2-3 afb1345*, and *afb2-1 afb1345* plants. **D**, 42-day old Col-0, *tir1-1 afb1345*, and *tir1-10 afb1345* plants.

Figure 1—figure supplement 3. Summary of phenotypes for mutant combinations. For the quantitative traits (Figure 1—figure supplement 4), the ranges for each of the phenotypes were divided into five bins, from "–" to "++++" in increasing severity. NA, Not applicable (due to embryo or seedling lethality); ND, not determined.

Figure 1—figure supplement 4. Shoot and root phenotypes of *tir1/afb* mutants. The seedlings/plants were grown in three batches (separated by dashed lines). Average

inflorescence height (**A**) and rosette diameter (**B**) of 42-day-old plants of the given genotypes (*n*=5 plants each). (**C**) Average numbers of inflorescence branches (≥ 1 cm) with the shades of gray distinguishing branches from primary, secondary, and tertiary inflorescences (*n*=5 plants each). (**D**) Average numbers of emerged lateral roots after five days on media lacking IAA then four days on media containing 100 nM IAA (*n*=12 seedlings). (**E**) Inhibition of root elongation assays. Seedlings were grown for five days on media lacking IAA then transferred to media containing 20 nM, 100 nM, 500 nM IAA, or DMSO-only control and grown for three days. Growth during the three days on media containing IAA is expressed as a percentage of the growth of the same genotype on control plates (*n*=12 seedlings for each treatment). The lines with an asterisk included a cross to an *afb4-2* containing line in their pedigrees, and alternate lines never exposed to the TILLING background were included in the third batch for five of the six such lines. The *afb123* line included in the first batch—and none of the others—exhibited a long-hypocotyl phenotype presumably acquired from the *afb4-2* line so it was excluded. The error bars indicate standard error of the mean (**A**–**D**) or the relative standard error of the ratio (**E**).

Figure 1—figure supplement 5. Embryonic root formation in *tir1/afb* mutants. **A**, representative seedlings of *tir1afb23* mutants with and without roots. **B**, four *tir1afb1245* seedlings with (left) and without roots (three on right), **C**, four rootless *tir1afb234* mutants. **D**, graph showing the percent of seedlings of different genotypes lacking roots (dark gray) or not germinating (light gray). The temperatures indicate the conditions in which the parents were grown, Percival growth chambers set to 17°C or 20°C or an

environmental room with temperatures between 22°C and 23°C. *, Different from 20°C, Fisher's exact test P<0.001. †, Different from tir1afb23, Fisher's exact test P<0.01.

Figure 3—figure supplement 1. Transgene complementing the *tir1afb12345* sextuple mutant. **A**, diagram of the Transfer-DNA region of pMP1855 containing genomic regions of *TIR1*, *AFB5*, and *AFB2* fused to *mOrange2*, *mCherry*, and *mCitrine*, respectively. BAR, Basta- (phosphinothricin-) resistance gene flanked by the *Agrobacterium nopaline synthase* promoter and terminator. **B**–**D**, confocal images of a globular-stage embryo from a *TO/5Ch/2Ci #d2/d2* plant detecting mOrange2 (**B**), mCherry, (**C**), and mCitrine (**D**). **E**–**F**, phenotypes of a 32-day-old WT Col-0 plant and a *tir1afb12345* plant hemizygous for the *TO/5Ch/2Ci #d2* transgene of the same age.

Figure 5—figure supplement 1. Comparison of *TIR1/AFB-mCitrine* lines. Roots of 5-day-old seedlings for two different lines are shown with a merged image of propidium iodide (magenta) and the fluorescent signal of mCitrine (yellow), mECFP (cyan), or mEGFP (green) on the left and fluorescent signal alone on the right. **A**, *TIR1-mCitrine#2*; **B**, *TIR1-mCitrine#4*; **C**, *AFB1-mCitrine#7*; **D**, *AFB1-mECFP#11*; **E**, *AFB2-mCitrine#3*; **F**, *AFB2-mCitrine#5*; **G**, *AFB3-mCitrine#1*; **H**, *AFB3-mEGFP#2*; **I**, *AFB4-mCitrine#1*; **J**, *AFB3-mCitrine#3*; **K**, *AFB5-mCitrine#23*; and **L**, *AFB3-mCitrine#9.* The first line for each gene is the same as shown in Figure 5. The same microscope settings for mCitrine detection in panels **A**–**B**, **E**–**G**, **J**–**K** (asterisks). The settings used for panels **C** and **L** were less sensitive (–) and those for panel **I** were more sensitive (+). Scale bars equal 25 µm. **M**, Sensitivities of *AFB4*-expressing transgenic lines to

picloram. Root elongation was measured for seedlings grown on media containing 20 µM picloram, expressed as a percentage of elongation on media lacking picloram. Lines *AFB4-mCitrine#3* and *AFB4-tdTomato#16* are more sensitive to picloram than WT indicating that the transgene is expressed at higher levels than the endogenous *AFB4* locus.

Supplementary File 1. List of databases for the sequences used in making the gene trees.

Supplementary File 2. List of primers used for cloning and genotyping.

Supplementary File 3. Nexus file for inferring the FBox-LRR family tree.

Supplementary File 4. Nexus file for inferring the TIR1+AFB1 tree.

REFERENCES

Alonso JM, Stepanova AN, Solano R, Wisman E, Ferrari S, Ausubel FM, Ecker JR. 2003. Five components of the ethylene-response pathway identified in a screen for *weak ethylene-insensitive* mutants in *Arabidopsis*. *Proc Natl Acad Sci U S A* **100**: 2992-2997.

Berleth T, Jürgens G. 1993. The Role of the *monopteros* Gene in Organizing the Basal Body Region of the *Arabidopsis* Embryo. *Development* **118**: 575-587.

Blilou I, Xu J, Wildwater M, Willemsen V, Paponov I, Friml J, Heidstra R, Aida M, Palme K, Scheres B. 2005. The PIN auxin efflux facilitator network controls growth and patterning in *Arabidopsis* roots. *Nature* **433**: 39-44.

Bowman JL, Briginshaw LN, Fisher TJ, Flores-Sandoval E. 2018. Something ancient and something neofunctionalized-evolution of land plant hormone signaling pathways. *Curr Opin Plant Biol* **47**: 64-72.

Brunoud G, Wells DM, Oliva M, Larrieu A, Mirabet V, Burrow AH, Beeckman T, Kepinski S, Traas J, Bennett MJ et al. 2012. A novel sensor to map auxin response and distribution at high spatio-temporal resolution. *Nature* **482**: 103-106.

Calderón Villalobos LI, Lee S, De Oliveira C, Ivetac A, Brandt W, Armitage L, Sheard LB, Tan X, Parry G, Mao H et al. 2012. A combinatorial TIR1/AFB-Aux/IAA co-receptor system for differential sensing of auxin. *Nat Chem Biol* **8**: 477-485.

Cheng Y, Dai X, Zhao Y. 2007. Auxin synthesized by the YUCCA flavin monooxygenases is essential for embryogenesis and leaf formation in *Arabidopsis*. *Plant Cell* **19**: 2430-2439.

Clark JW, Donoghue PCJ. 2018. Whole-Genome Duplication and Plant Macroevolution. *Trends Plant Sci* **23**: 933-945.

Clough SJ, Bent AF. 1998. Floral dip: a simplified method for *Agrobacterium*-mediated transformation of *Arabidopsis thaliana*. *Plant J* **16**: 735-743.
Crawford BC, Sewell J, Golembeski G, Roshan C, Long JA, Yanofsky MF. 2015. Genetic control of distal stem cell fate within root and embryonic meristems. *Science* **347**: 655-659.
Delker C, Poschl Y, Raschke A, Ullrich K, Ettingshausen S, Hauptmann V, Grosse I, Quint M. 2010. Natural variation of transcriptional auxin response networks in *Arabidopsis thaliana*. *Plant Cell* **22**: 2184-2200.
Dezfulian MH, Jalili E, Roberto DK, Moss BL, Khoo K, Nemhauser JL, Crosby WL. 2016. Oligomerization of SCFTIR1 Is Essential for Aux/IAA Degradation and Auxin Signaling in Arabidopsis. *PLoS Genet* **12**: e1006301.
Dharmasiri N, Dharmasiri S, Weijers D, Lechner E, Yamada M, Hobbie L, Ehrismann JS, Jürgens G, Estelle M. 2005. Plant development is regulated by a family of auxin receptor F box proteins. *Dev Cell* **9**: 109-119.
Dindas J, Scherzer S, Roelfsema MRG, von Meyer K, Muller HM, Al-Rasheid KAS, Palme K, Dietrich P, Becker D, Bennett MJ et al. 2018. AUX1-mediated root hair auxin influx governs SCF(TIR1/AFB)-type Ca(2+) signaling. *Nat Commun* **9**: 1174.
Edwards K, Johnstone C, Thompson C. 1991. A simple and rapid method for the preparation of plant genomic DNA for PCR analysis. *Nucleic Acids Res* **19**: 1349.
Fendrych M, Akhmanova M, Merrin J, Glanc M, Hagihara S, Takahashi K, Uchida N, Torii KU, Friml J. 2018. Rapid and reversible root growth inhibition by TIR1 auxin signalling. *Nat Plants* **4**: 453-459.
Franklin KA, Quail PH. 2010. Phytochrome functions in *Arabidopsis* development. *J Exp Bot* **61**: 11-24.
Friml J, Vieten A, Sauer M, Weijers D, Schwarz H, Hamann T, Offringa R, Jürgens G. 2003. Efflux-dependent auxin gradients establish the apical-basal axis of *Arabidopsis*. *Nature* **426**: 147-153.
Goodstein DM, Shu S, Howson R, Neupane R, Hayes RD, Fazo J, Mitros T, Dirks W, Hellsten U, Putnam N et al. 2012. Phytozome: a comparative platform for green plant genomics. *Nucleic Acids Res* **40**: D1178-1186.
Griesbeck O, Baird GS, Campbell RE, Zacharias DA, Tsien RY. 2001. Reducing the environmental sensitivity of yellow fluorescent protein. Mechanism and applications. *J Biol Chem* **276**: 29188-29194.
Hamann T, Benková E, Bäurle I, Kientz M, Jürgens G. 2002. The *Arabidopsis BODENLOS* gene encodes an auxin response protein inhibiting MONOPTEROS-mediated embryo patterning. *Genes Dev* **16**: 1610-1615.
Hamann T, Mayer U, Jürgens G. 1999. The auxin-insensitive *bodenlos* mutation affects primary root formation and apical-basal patterning in the *Arabidopsis* embryo. *Development* **126**: 1387-1395.
Hardtke CS, Berleth T. 1998. The *Arabidopsis* gene *MONOPTEROS* encodes a transcription factor mediating embryo axis formation and vascular development. *EMBO J* **17**: 1405-1411.
Heisler MG, Ohno C, Das P, Sieber P, Reddy GV, Long JA, Meyerowitz EM. 2005. Patterns of auxin transport and gene expression during primordium development

revealed by live imaging of the *Arabidopsis* inflorescence meristem. *Curr Biol* **15**: 1899-1911.
Hori K, Maruyama F, Fujisawa T, Togashi T, Yamamoto N, Seo M, Sato S, Yamada T, Mori H, Tajima N et al. 2014. *Klebsormidium flaccidum* genome reveals primary factors for plant terrestrial adaptation. *Nat Commun* **5**: 3978.
Johnson MT, Carpenter EJ, Tian Z, Bruskiewich R, Burris JN, Carrigan CT, Chase MW, Clarke ND, Covshoff S, Depamphilis CW et al. 2012. Evaluating methods for isolating total RNA and predicting the success of sequencing phylogenetically diverse plant transcriptomes. *PLoS One* **7**: e50226.
Jones-Rhoades MW, Bartel DP. 2004. Computational identification of plant microRNAs and their targets, including a stress-induced miRNA. *Mol Cell* **14**: 787-799.
Kurihara D, Mizuta Y, Sato Y, Higashiyama T. 2015. ClearSee: a rapid optical clearing reagent for whole-plant fluorescence imaging. *Development* **142**: 4168-4179.
Lavy M, Estelle M. 2016. Mechanisms of auxin signaling. *Development* **143**: 3226-3229.
Lee S, Sundaram S, Armitage L, Evans JP, Hawkes T, Kepinski S, Ferro N, Napier RM. 2014. Defining binding efficiency and specificity of auxins for SCF(TIR1/AFB)-Aux/IAA co-receptor complex formation. *ACS Chem Biol* **9**: 673-682.
Liao CY, Smet W, Brunoud G, Yoshida S, Vernoux T, Weijers D. 2015. Reporters for sensitive and quantitative measurement of auxin response. *Nat Methods* **12**: 207-210, 202 p following 210.
Ligerot Y, de Saint Germain A, Waldie T, Troadec C, Citerne S, Kadakia N, Pillot JP, Prigge M, Aubert G, Bendahmane A et al. 2017. The pea branching *RMS2* gene encodes the PsAFB4/5 auxin receptor and is involved in an auxin-strigolactone regulation loop. *PLoS Genet* **13**: e1007089.
Lynch M, Conery JS. 2003. The evolutionary demography of duplicate genes. *J Struct Funct Genomics* **3**: 35-44.
Maddison WP, Maddison DR. 2018. Mesquite: a modular system for evolutionary analysis. Version 3.51.
Matasci N, Hung LH, Yan Z, Carpenter EJ, Wickett NJ, Mirarab S, Nguyen N, Warnow T, Ayyampalayam S, Barker M et al. 2014. Data access for the 1,000 Plants (1KP) project. *Gigascience* **3**: 17.
Morris JL, Puttick MN, Clark JW, Edwards D, Kenrick P, Pressel S, Wellman CH, Yang Z, Schneider H, Donoghue PCJ. 2018. The timescale of early land plant evolution. *Proc Natl Acad Sci U S A* **115**: E2274-E2283.
Mutte SK, Kato H, Rothfels C, Melkonian M, Wong GK, Weijers D. 2018. Origin and evolution of the nuclear auxin response system. *Elife* **7**.
Navarro L, Dunoyer P, Jay F, Arnold B, Dharmasiri N, Estelle M, Voinnet O, Jones JD. 2006. A plant miRNA contributes to antibacterial resistance by repressing auxin signaling. *Science* **312**: 436-439.
Notredame C, Higgins DG, Heringa J. 2000. T-Coffee: A novel method for fast and accurate multiple sequence alignment. *J Mol Biol* **302**: 205-217.
Palovaara J, de Zeeuw T, Weijers D. 2016. Tissue and Organ Initiation in the Plant Embryo: A First Time for Everything. *Annu Rev Cell Dev Biol* **32**: 47-75.
Panchy N, Lehti-Shiu M, Shiu SH. 2016. Evolution of Gene Duplication in Plants. *Plant Physiol* **171**: 2294-2316.

Parry G, Calderón-Villalobos LI, Prigge M, Péret B, Dharmasiri S, Itoh H, Lechner E, Gray WM, Bennett M, Estelle M. 2009. Complex regulation of the TIR1/AFB family of auxin receptors. *Proc Natl Acad Sci U S A* **106**: 22540-22545.
Prigge MJ, Greenham K, Zhang Y, Santner A, Castillejo C, Mutka AM, O'Malley RC, Ecker JR, Kunkel BN, Estelle M. 2016. The *Arabidopsis* Auxin Receptor F-Box Proteins AFB4 and AFB5 Are Required for Response to the Synthetic Auxin Picloram. *G3 (Bethesda)* **6**: 1383-1390.
Prigge MJ, Otsuga D, Alonso JM, Ecker JR, Drews GN, Clark SE. 2005. Class III homeodomain-leucine zipper gene family members have overlapping, antagonistic, and distinct roles in Arabidopsis development. *Plant Cell* **17**: 61-76.
Pucciariello O, Legris M, Costigliolo Rojas C, Iglesias MJ, Hernando CE, Dezar C, Vazquez M, Yanovsky MJ, Finlayson SA, Prat S et al. 2018. Rewiring of auxin signaling under persistent shade. *Proc Natl Acad Sci U S A* **115**: 5612-5617.
Rademacher EH, Lokerse AS, Schlereth A, Llavata-Peris CI, Bayer M, Kientz M, Freire Rios A, Borst JW, Lukowitz W, Jürgens G et al. 2012. Different auxin response machineries control distinct cell fates in the early plant embryo. *Dev Cell* **22**: 211-222.
Rambaut A. 2018. FigTree v1.4.4 (http://tree.bio.ed.ac.uk/software/figtree/).
Remington DL, Vision TJ, Guilfoyle TJ, Reed JW. 2004. Contrasting modes of diversification in the *Aux/IAA* and *ARF* gene families. *Plant Physiol* **135**: 1738-1752.
Rensing SA, Lang D, Zimmer AD, Terry A, Salamov A, Shapiro H, Nishiyama T, Perroud PF, Lindquist EA, Kamisugi Y et al. 2008. The *Physcomitrella* genome reveals evolutionary insights into the conquest of land by plants. *Science* **319**: 64-69.
Robert HS, Grunewald W, Sauer M, Cannoot B, Soriano M, Swarup R, Weijers D, Bennett M, Boutilier K, Friml J. 2015. Plant embryogenesis requires AUX/LAX-mediated auxin influx. *Development* **142**: 702-711.
Ronquist F, Teslenko M, van der Mark P, Ayres DL, Darling A, Hohna S, Larget B, Liu L, Suchard MA, Huelsenbeck JP. 2012. MrBayes 3.2: efficient Bayesian phylogenetic inference and model choice across a large model space. *Syst Biol* **61**: 539-542.
Ruegger M, Dewey E, Gray WM, Hobbie L, Turner J, Estelle M. 1998. The TIR1 protein of *Arabidopsis* functions in auxin response and is related to human SKP2 and yeast grr1p. *Genes Dev* **12**: 198-207.
Ruegger M, Dewey E, Hobbie L, Brown D, Bernasconi P, Turner J, Muday G, Estelle M. 1997. Reduced naphthylphthalamic acid binding in the *tir3* mutant of Arabidopsis is associated with a reduction in polar auxin transport and diverse morphological defects. *Plant Cell* **9**: 745-757.
Schindelin J, Arganda-Carreras I, Frise E, Kaynig V, Longair M, Pietzsch T, Preibisch S, Rueden C, Saalfeld S, Schmid B et al. 2012. Fiji: an open-source platform for biological-image analysis. *Nat Methods* **9**: 676-682.
Schneider CA, Rasband WS, Eliceiri KW. 2012. NIH Image to ImageJ: 25 years of image analysis. *Nat Methods* **9**: 671-675.
Schranz ME, Mitchell-Olds T. 2006. Independent ancient polyploidy events in the sister families Brassicaceae and Cleomaceae. *Plant Cell* **18**: 1152-1165.

Shaner NC, Campbell RE, Steinbach PA, Giepmans BN, Palmer AE, Tsien RY. 2004. Improved monomeric red, orange and yellow fluorescent proteins derived from *Discosoma* sp. red fluorescent protein. *Nat Biotechnol* **22**: 1567-1572.

Shaner NC, Lin MZ, McKeown MR, Steinbach PA, Hazelwood KL, Davidson MW, Tsien RY. 2008. Improving the photostability of bright monomeric orange and red fluorescent proteins. *Nat Methods* **5**: 545-551.

Stepanova AN, Robertson-Hoyt J, Yun J, Benavente LM, Xie DY, Doležal K, Schlereth A, Jürgens G, Alonso JM. 2008. *TAA1*-mediated auxin biosynthesis is essential for hormone crosstalk and plant development. *Cell* **133**: 177-191.

Strasser B, Sánchez-Lamas M, Yanovsky MJ, Casal JJ, Cerdán PD. 2010. *Arabidopsis thaliana* life without phytochromes. *Proc Natl Acad Sci U S A* **107**: 4776-4781.

Ursache R, Andersen TG, Marhavy P, Geldner N. 2018. A protocol for combining fluorescent proteins with histological stains for diverse cell wall components. *Plant J* **93**: 399-412.

Vidal EA, Araus V, Lu C, Parry G, Green PJ, Coruzzi GM, Gutiérrez RA. 2010. Nitrate-responsive miR393/*AFB3* regulatory module controls root system architecture in *Arabidopsis thaliana*. *Proc Natl Acad Sci U S A* **107**: 4477-4482.

Walsh TA, Neal R, Merlo AO, Honma M, Hicks GR, Wolff K, Matsumura W, Davies JP. 2006. Mutations in an auxin receptor homolog AFB5 and in SGT1b confer resistance to synthetic picolinate auxins and not to 2,4-dichlorophenoxyacetic acid or indole-3-acetic acid in Arabidopsis. *Plant Physiol* **142**: 542-552.

Wang R, Zhang Y, Kieffer M, Yu H, Kepinski S, Estelle M. 2016. HSP90 regulates temperature-dependent seedling growth in *Arabidopsis* by stabilizing the auxin co-receptor F-box protein TIR1. *Nat Commun* **7**: 10269.

Wickett NJ, Mirarab S, Nguyen N, Warnow T, Carpenter E, Matasci N, Ayyampalayam S, Barker MS, Burleigh JG, Gitzendanner MA et al. 2014. Phylotranscriptomic analysis of the origin and early diversification of land plants. *Proc Natl Acad Sci U S A* **111**: E4859-4868.

Wright RC, Zahler ML, Gerben SR, Nemhauser JL. 2017. Insights into the Evolution and Function of Auxin Signaling F-Box Proteins in *Arabidopsis thaliana* Through Synthetic Analysis of Natural Variants. *Genetics* **207**: 583-591.

Xie Y, Wu G, Tang J, Luo R, Patterson J, Liu S, Huang W, He G, Gu S, Li S et al. 2014. SOAPdenovo-Trans: de novo transcriptome assembly with short RNA-Seq reads. *Bioinformatics* **30**: 1660-1666.

Yu H, Zhang Y, Moss BL, Bargmann BO, Wang R, Prigge M, Nemhauser JL, Estelle M. 2015. Untethering the TIR1 auxin receptor from the SCF complex increases its stability and inhibits auxin response. *Nat Plants* **1**.

Zhou R, Benavente LM, Stepanova AN, Alonso JM. 2011. A recombineering-based gene tagging system for Arabidopsis. *Plant J* **66**: 712-723.

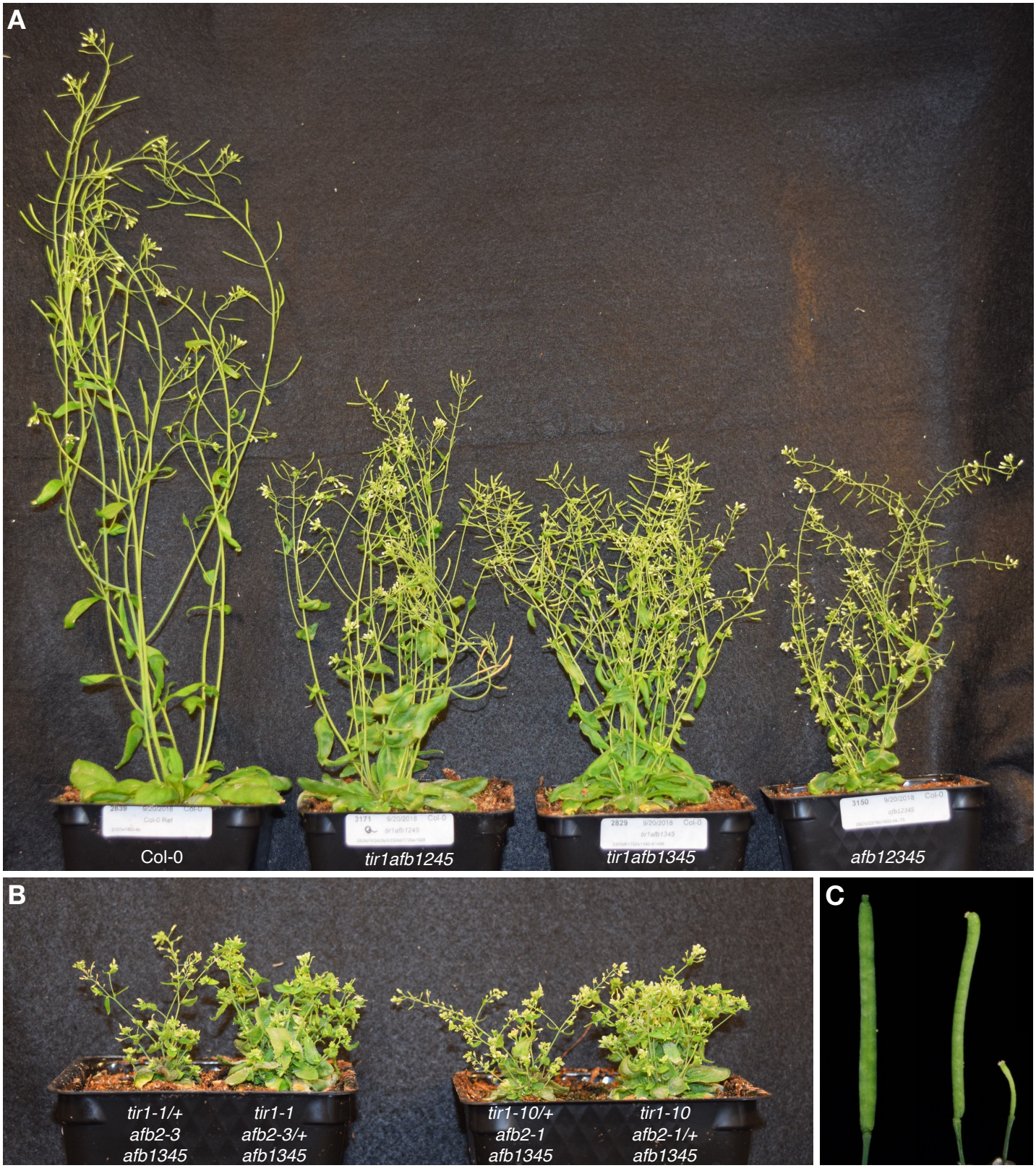

Figure 1. *tir1/afb* mutant lines exhibit a range of shoot phenotypes. (**A**) The viable quintuple mutants, *tir1afb1245, tir1afb1345*, and *afb12345,* are each approximately half the height of Col-0 WT, but differ in other phenotypes. Note the curved silique tips of the *tir1afb1245* mutant (indicative of gynoecium defects) and the short siliques (due to poor fertility) of the *afb12345* mutant. (**B**) Lines with only one *TIR1+* or one *AFB2+* allele display similar phenotypes regardless of the mutant *tir1* and *afb2* alleles: left to right, *tir1-1/+ afb2-3 afb1345*, *tir1-1 afb2-3/+ afb1345*, *tir1-10/+ afb2-1 afb1345*, and *tir1-10 afb2-1/+ afb1345*. (**C**) Normal siliques (Col-0, left) have two valves containing developing seeds while siliques of *afb2/+ tir1afb35* plants usually lack one (middle) or both valves (right). Plants were grown for 42 days (A and B) or 39 days (C) at 22°C and 16h daylength.

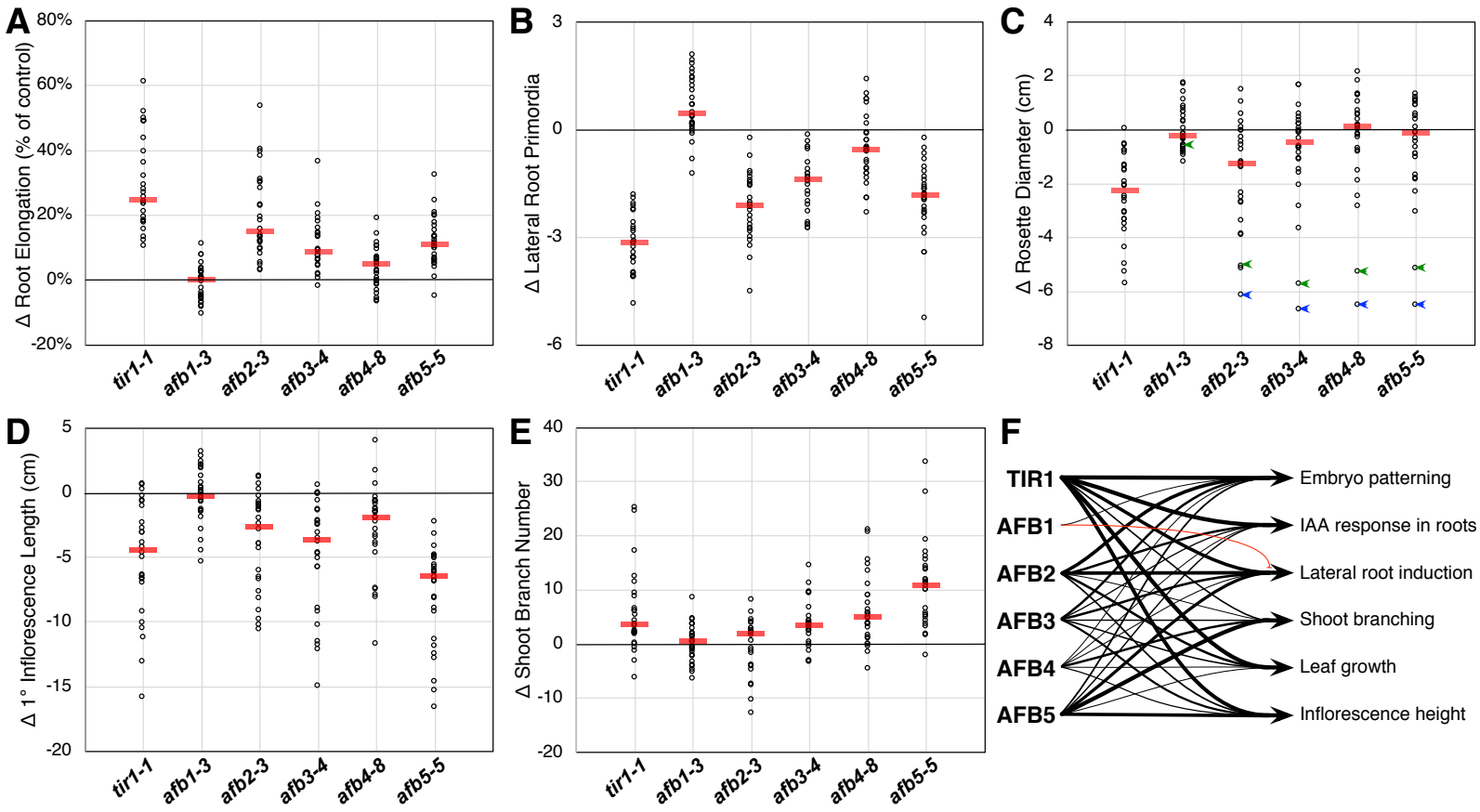

Figure 2. Relative *TIR1/AFB* gene effects. For each of the five phenotype measurements (Figure 1—figure supplement 4), the normalized mean for each genotype with the given mutation was subtracted from the normalized mean for the corresponding genotype lacking that mutation and plotted (circles). The red bars indicate the median difference attributable to the given mutation. (**A**) Effects of each mutation on IAA-inhibition of root elongation. For each genotype, twelve five-day-old seedings were transferred and grown for three days on media containing 100 nM IAA, and their average growth was divided by that of twelve seedlings grown on media lacking added auxin. (**B**) Effects of each mutation on auxin-induced lateral root production. Twelve five-day-old seedings for each genotype were grown for four days on media containing 100 nM IAA and the numbers of emerged lateral roots were counted. (**C**) Effects of each mutation on the average rosette diameters of five 42-day old plants. The blue arrowheads indicate difference in phenotypes between the *afb2345* quadruple mutant and the four triple mutants, and the green arrowheads indicate those for the *afb12345* quintuple mutant and the five quadruple mutants. (**D**) Effects of each mutation on the average height of the primary inflorescences for five 42-day old plants. (**E**) Effects of each mutation on the average number of inflorescence branches (≥1 cm) on five 42-day old plants. (**F**) Representation of the relative gene effects based on panels **A** through **E** plus embryo phenotypes (below). The line weights reflect the relative importance for each gene's roles. The red line with the bar end indicates the antagonistic role observed for *AFB1*.

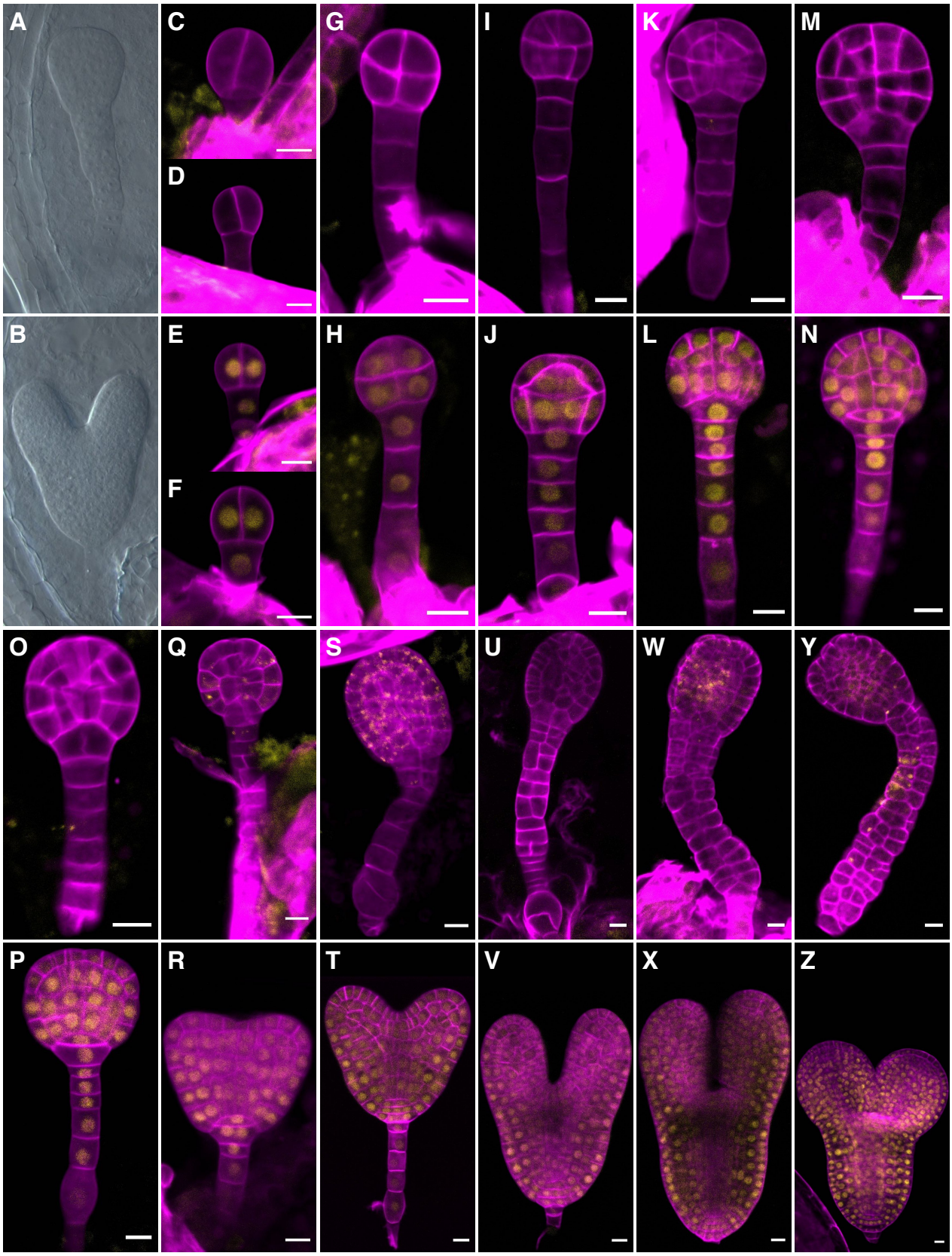

Figure 3. Embryo-lethal phenotypes of *tir1/afb* mutant lines. Approximately one-quarter of the chloral-hydrate-cleared embryos from siliques of *afb2/+ tir1afb35* plants did not produce cotyledon primordia and have over-proliferated suspensors (**A**) while the remaining siblings from the same silique appear normal (**B**). Embryos from *TO/5Ch/2Ci#d2/+ tir1afb12345* (**C**–**O, R**–**Z**) and *TO/5Ch/2Ci#d1/+ tir1afb12345* (**P**–**Q**) plants were fixed, stained with SR2200 (cell walls, magenta), and scanned for fluorescence from the AFB2-mCitrine fusion protein (yellow). The embryos in panels **C**, **D**, **G**, **I**, **K**, **M**, **O**, **Q**, **S**, **U**, **W**, and **Y** are sextuple mutants lacking mCitrine signal while those in **E**, **F**, **H**, **J**, **L**, **N**, **P**, **R**, **T**, **V**, **X**, and **Z** are complemented siblings. The embryo stages are 2-cell (**C**–**F**), 8-cell (octant) (**G**–**H**), 16-cell (dermatogen) (**I**–**J**), early globular (**K**–**L**), late globular (**M**–**P**), late transition (**Q**–**R**), heart (**S**–**T**), torpedo (**U**–**X**), and bent cotyledon (**Y**–**Z**). The cytoplasmic signal in panels **S**, **W**, and **Y** likely represents autofluorescence of senescing cells.

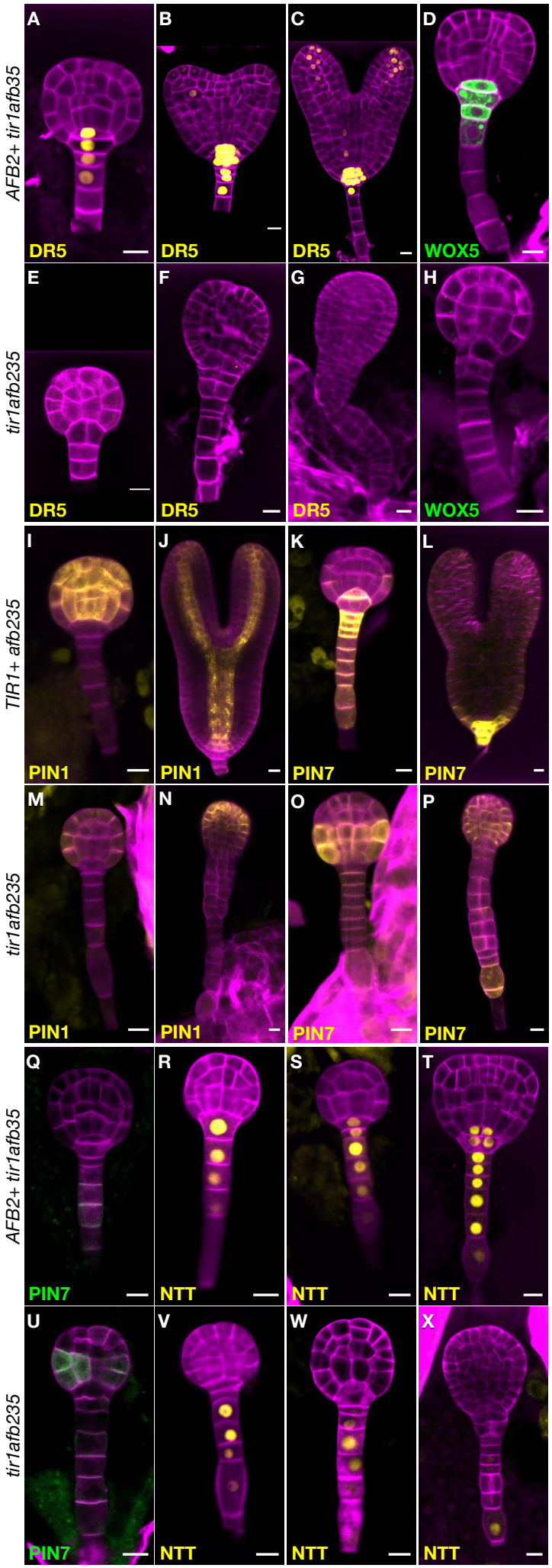

Figure 4. Marker gene expression in the *tir1afb235* embryos. Fluorescence in embryos from both *afb2/+ tir1afb35 DR5rev:3×Venus-N7* (**A**–**C, E**–**G**) and *afb2/+ tir1afb35 WOX5:GFP$_{ER}$* (**D**, **H**) markers was present in phenotypically normal siblings (**A**–**D**) but absent in abnormal (presumed *tir1afb235*) embryos (**E**–**H**). Fluorescence in embryos from *tir1/+afb235 PIN1-Venus* plants: normal-phenotype globular embryo (**I**), normal-phenotype torpedo-stage embryo (**J**), mutant-phenotype globular embryo (**M**) and later-stage embryo (**N**). Progeny of *tir1/+ afb235 PIN7-Venus* or *afb2/+ tir1afb35 PIN7-GFP* plants: phenotypically normal globular embryos (**K**, **Q**) mutant globular embryos (**O**, **U**), and normal (**L**) and mutant (**P**) torpedo-stage embryos. Progeny of *afb2/+ tir1afb35 NTT-YPet* plants: normal-phenotype globular- (**R**–**S**) and transition- (**T**) stage embryos, and mutant embryos (**V**–**X**). Scale bars: 10 μm.

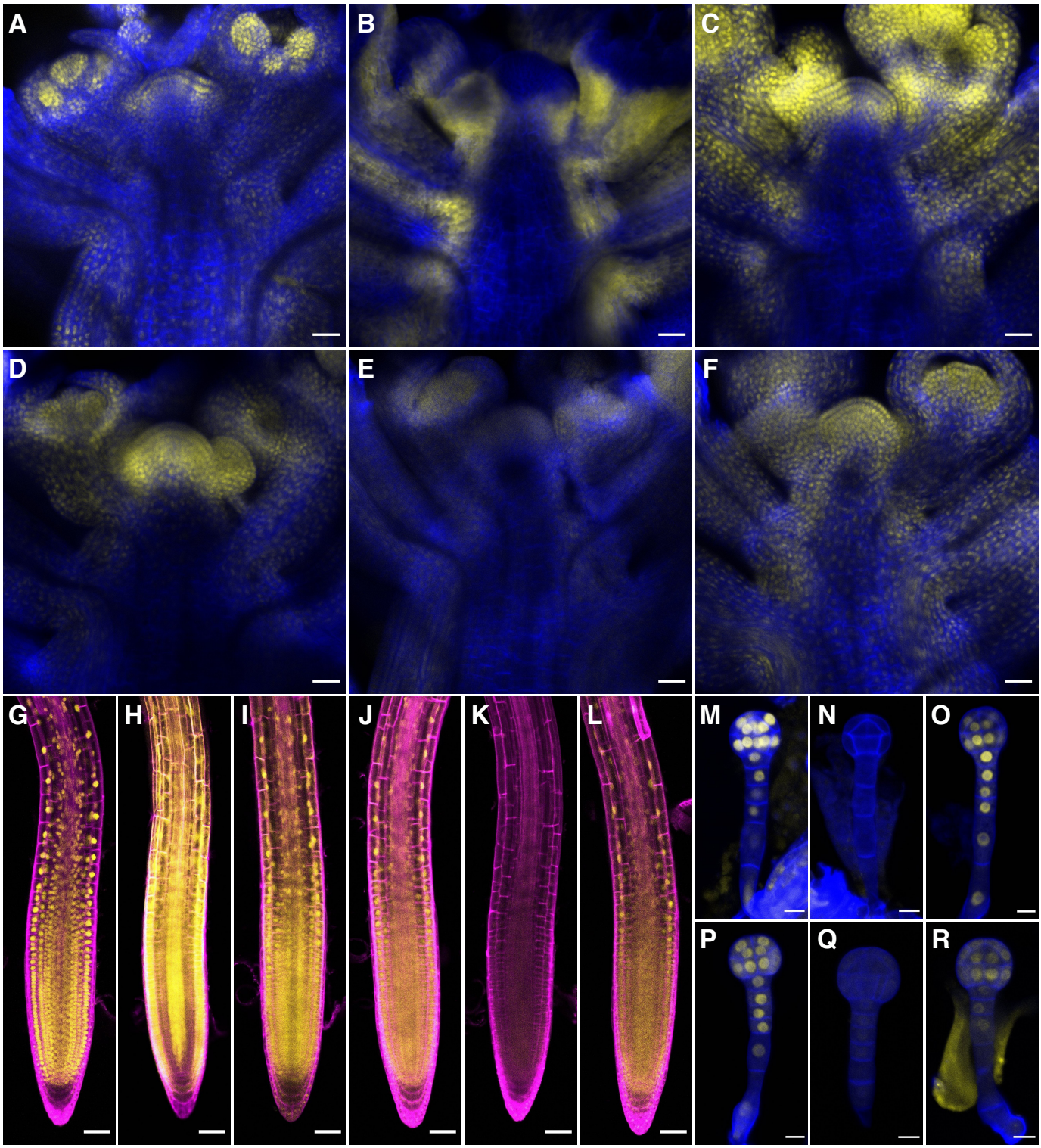

Figure 5. Expression of *TIR1/AFB-mCitrine* fusions. mCitrine signal is shown as yellow in all panels, and cell walls were stained with Calcofluor White M2R (blue; **A**–**F**), propidium iodide (magenta; **G**–**L**), and SCRI Renaissance 2200 (blue; **M**–**R**). Confocal images of inflorescence apices from 4-week-old plants containing the specified *TIR1/AFB-mCitrine* transgenes in the corresponding single-mutant background: **A**, *tir1-10 TIR1-mCitrine#2*; **B**, *afb1-3 AFB1-mCitrine#7*; **C**, *afb2-3 AFB2-mCitrine#3*; **D**, *afb3-4 AFB3-mCitrine#1*; **E**, *afb4-8 AFB4-mCitrine#3*; and **F**, *afb5-5 AFB5-mCitrine#19*. Confocal images of roots of *tir1-10 TIR1-mCitrine#2* (**G**), *afb1-3 AFB1-mCitrine#7* (**H**), *afb2-3 AFB2-mCitrine#3* (**I**), *afb3-4 AFB3-mCitrine#1* (**J**), *afb4-8 AFB4-mCitrine#1* (**K**), and *afb5-5 AFB5-mCitrine#23* (**L**) 5-day old seedlings. Images in panels **G** and **J**–**L** used similar microscope settings while those in panels **H** and **I** used less sensitive settings. Confocal images of dermatogen or early globular embryos of *tir1-10 TIR1-mCitrine#2* (**M**), *afb1-3 AFB1-mCitrine#7* (**N**), *afb2-3 AFB2-mCitrine#3* (**O**), *afb3-4 AFB3-mCitrine#1* (**P**), *afb4-8 AFB4-mCitrine#3* (**Q**), and *afb5-5 AFB5-mCitrine#19* (**R**) plants. Scale bars equal 25 µm (**A**–**F**), 50 µm (**G**–**L**), and 10 µm (**M**–**R**).